ADVANCED ELECTRONIC MATERIALS
www.advelectronicmat.de

Photocurrent, Photovoltage, and Rectification in Large-Area Bilayer Molecular Electronic Junctions

*Scott R. Smith and Richard L. McCreery**

Bilayer donor–acceptor molecular junctions are successfully fabricated with active layer thickness <15 nm to study the mechanism of photo-induced charge transport. The bilayer devices exhibit lifetimes greater than 1 h with laser irradiation, and a strong dependence of the sign and magnitude of the photovoltage and photocurrent on structure and order of the molecular layers. A distinct feature of the bilayer structure is covalent bonding between the donor and acceptor molecular layers, which permits simultaneous absorption and charge separation across a covalent heterojunction. In addition to providing probes of internal energy levels and charge transport in molecular junctions, photo-induced currents and voltages may potentially be useful in light-weight, durable, and flexible photodetectors.

A central objective of the field of molecular electronics (ME) is realization of novel electronic functions in solid-state devices, which are difficult or impossible to achieve with conventional electronic materials. Interactions of light with molecular devices not only provide important diagnostics of structure and internal energy levels, but also may be exploited for photodetection and light emission. We report here a bilayer molecular junction (MJ) with electron donor and acceptor moieties with a combined thickness of <15 nm, both of which absorb UV–vis light and are covalently bonded to partially transparent carbon contacts. The bilayer structure not only introduces an organic–organic interface but also permits photon-stimulated unidirectional electron transport to yield a photocurrent at zero bias and a photovoltage at open circuit. A bilayer junction of anthraquinone (AQ) and bisthienylbenzene (BTB) illuminated by continuum or laser UV–vis light yields photocurrents (PCs) 15× and photovoltages 50× larger than those observed for single-layer devices. The photoresponses are independent of illumination direction and determined by the relative energies of the molecular orbitals in the two layers. The distinct properties of bilayer MJs compared with previous single-molecular layer devices are discussed in terms of the optical transitions and charge transport mechanisms enabled in the bilayer structure.

Research in ME involves studying the electrical response of single molecules or assemblies of molecules in parallel between two electrode contacts, referred to as a "molecular junction (MJ)".[1] A MJ may employ a single organic substituent or repeating units (e.g., an oligomer) to achieve variations in the electronic response depending on structure and molecular layer thickness.[2] Alternatively, MJs may contain two or more molecular layers differing in structure and orbital energies to create multilayered MJs with novel electronic behaviors. As examples, bilayer MJs integrate electron donor and acceptor layers in a single oligomer to achieve an electronic rectifier,[2e,3] and trilayers that further incorporate mobile Li^+ ions can act as a redox active memory or energy storage device with total thickness <15 nm.[4] Understanding the relationship between the structure, orbital energies, and electronic behavior of both single and multilayer MJs is paramount to engineering new ME devices for a potentially broad range of electronic functions.

In addition to optical spectroscopy used to verify MJ structure, illumination of MJs can produce an electronic response,[5] and current through a MJ can result in light emission.[6] The single-component MJs studied to date show relatively weak photoeffects such as internal photoemission (IPE)[5a,e,f] and conductance changes,[5b] due in part to weak optical absorption by the thin molecular layer. We recently reported PCs at zero bias for eight single-component carbon/molecule/carbon MJs with varying molecular structure. While the PCs correlated with transport properties across a range of structures, the external quantum efficiencies were small, in the range of 10^{-5} to 10^{-4} photoelectrons/incident photon.[7]

In contrast to symmetric current density versus bias voltage (*JV*) behavior observed with single-component layers, bilayer MJs with an electron accepting layer that is subsequently overlaid with an electron donating layer between symmetric sp^2 carbon contacts exhibit nonlinear, asymmetric *JV* responses with rectification ratios (*RR*) of 10–290 for different bilayer combinations.[3] The bilayer introduced asymmetry into a previously symmetric single-layer device, and the rectification direction could be reversed by changing the order of the molecular layers. The current investigation examines photoeffects in molecular bilayers (10–15 nm total thickness) with two main motivations. First, the photoresponse of the MJs should reveal relationships between internal energy levels of both the molecules and the associated contacts in completed, functioning MJs. Second, sensitivity to light is a potentially useful function in ME, and bilayer devices may be good candidates for photodetectors. Unlike the common semiconductor photodetectors,

Dr. S. R. Smith, Prof. R. L. McCreery
Department of Chemistry
University of Alberta
11227 Saskatchewan Drive, Edmonton, Alberta T6G 2G2, Canada
E-mail: richard.mccreery@ualberta.ca

The ORCID identification number(s) for the author(s) of this article can be found under https://doi.org/10.1002/aelm.201800093.

DOI: 10.1002/aelm.201800093

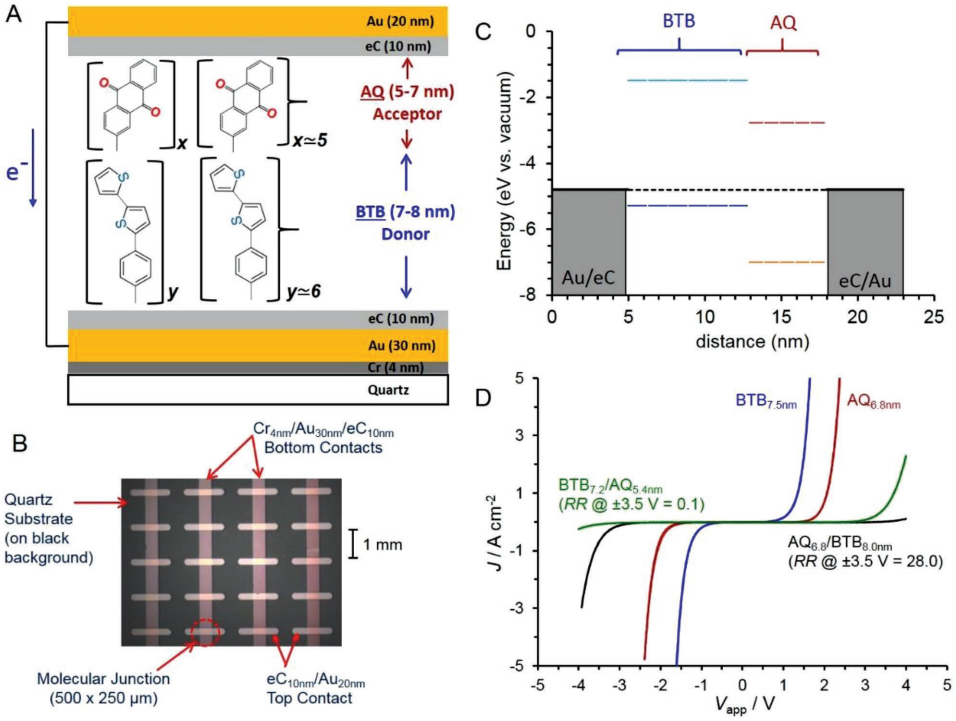

Figure 1. A) Schematic of carbon/bilayer/carbon MJ (*x* and *y* indicate number of oligomer units from AFM-determined thicknesses[3]) of AQ and BTB. B) Image of an array of 500 × 250 μm molecular junctions on a quartz substrate. C) Energy level diagram for a BTB–AQ bilayer junction based on DFT of free molecules and ignoring possible perturbations by contact to the electrodes. D) Average *JV* curves for minimum of ten junctions each of AQ (red curve), BTB (blue curve), AQ–BTB (black curve), and BTB–AQ (green curve); scan rate 1000 V s^{-1} in vacuum (<1 × 10^{-5} torr).

the molecular photoresponse covers a narrower and tunable wavelength range, which is readily varied by changes in molecular structure. The bilayer structure under study is shown in **Figure 1**A and is composed of an AQ (an electron acceptor) layer and a second layer of an electron donor, BTB. Although employing an electron donor–acceptor pair such as AQ and BTB is analogous to organic photovoltaics,[8] the current MJs are significantly thinner (by factors of 10 to 100×) and have different transport mechanisms than the activated hopping common in organic thin film devices. Electrochemical and spectroscopic characterization of the bilayer devices will be discussed in terms of structure and transport mechanism, with possible applications in ME and photonics.

MJs of single-component layers of AQ and BTB, along with bilayer devices of BTB–AQ and AQ–BTB, were fabricated on patterned quartz/Cr_4/Au_{30}/C_{10} substrates with C_{10}/Au_{20} top contacts using established techniques[3,6a,9] to achieve arrays of MJs (Figure 1B, subscripts indicate layer thicknesses in nm determined with atomic force microscopy (AFM)). Figure 1C displays a schematic energy level diagram for the bilayer BTB–AQ molecular device under zero bias showing the highest occupied (HOMO) and lowest unoccupied molecular orbitals (LUMO) of the BTB and AQ bilayer MJs (estimated with Gaussian 09 [B3LYP/6-31G(d)] for the free molecules) with the electron beam deposited carbon (eC) electrode contacts. The eC Fermi levels are assumed equal to –4.8 eV versus vacuum, as determined previously.[9,10]

Figure 1D displays the average *JV* behavior collected under vacuum of the four MJ structures in the present study with the observed *RR* values ($RR \equiv |J_{-3.5\ V}/J_{+3.5\ V}|$) of the bilayer MJs. All *JV* curves were observed to be similar to those previously reported,[3,9,11] independent of scan rate in the bias region studied, and stable for at least thousands of *JV* scans. The bilayer *JV* curves require larger applied bias to achieve current densities similar to the single-layer MJs due mainly to increased thickness. As noted previously, the direction of rectification for bilayer AQ–BTB MJs was determined by the order of the molecular layers, with the larger current densities occurring when the electron acceptor (AQ) is biased negatively.[3] In the absence of light, the rectification persists for temperatures of 7 to 200 K, then becomes more pronounced above 200 K. The mechanism was attributed to the relative magnitudes of the injection barriers of the donor and acceptor molecules under bias.[3]

Absorbance spectra of AQ, BTB, AQ–BTB, and BTB–AQ are shown in **Figure 2**A for nonpatterned quartz/Cr_4/Au_{25}/eC_{10} substrates to determine the single and bilayer optical absorption. The single layer of AQ exhibits a main absorption peak centered at 259 nm and a second smaller peak at 336 nm,[9] while single layers of BTB exhibit strong absorption at 360 nm with a small feature at 257 nm. Absorption spectra of the AQ–BTB and BTB–AQ bilayers reveal two bands characteristic of the main peak of BTB and AQ, respectively, suggesting successful incorporation of both substituents in the bilayer with weak intermolecular electronic coupling. However, an additional, lower intensity band was observed in each of the bilayer absorption spectra at longer wavelengths, ≈500 to 800 nm, consistent with intramolecular charge transfer bands of an electron from the BTB HOMO directly to the AQ LUMO, which are predicted to occur by density functional theory (DFT) in this region for

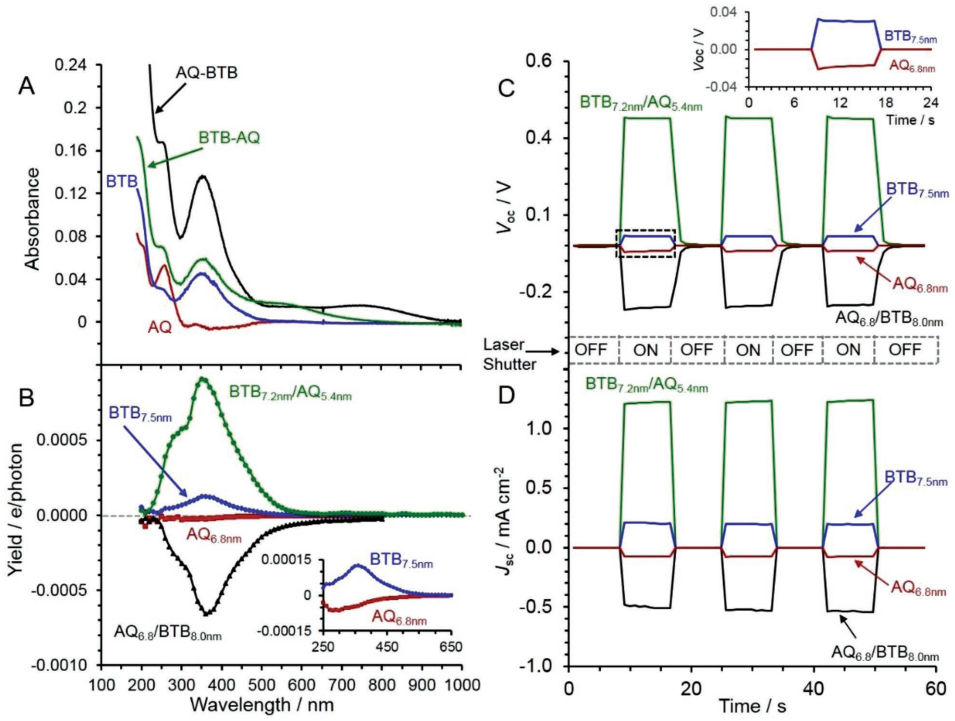

Figure 2. A) UV–vis absorbance of Au/eC modified with AQ (red curve), BTB (blue curve), AQ–BTB (black curve), and BTB–AQ (green curve) after subtraction of substrate spectra.[9] B) PC yield versus wavelength of molecular junctions containing AQ (red curve), BTB (blue curve), AQ–BTB (black curve), and BTB–AQ (green curve). C) Open-circuit voltage (V_{oc}) in response to a 407 nm, 10 mW laser. Short-circuit current density (J_{sc}) for same MJs, same colors as panels (A) and (B).

both of the bilayer systems (as described in the Supporting Information).

PC yield is defined as the number of photoelectrons in the external circuit (see Figures S1 and S2, Supporting Information) divided by the number of photons incident on the MJ and plotted versus photon wavelength for single and bilayer devices in Figure 2B. Positive PC yield corresponds to electron flow from the top to the bottom electrode in the external circuit (see arrow at left of Figure 1A). The low yields in Figure 2B are due in part to the low electrode transparency (13%) and short absorption path length in the molecular layer (≈15 nm). The internal efficiency defined as the number of photoelectrons generated per photon absorbed in the molecular layer is significantly higher, up to 12% for the range of conditions examined. The maxima observed in PC yield for the single layers of BTB and AQ were centered at 360 and 300 nm, respectively (Figure 2B inset), and correspond approximately to the observed absorbance peak maxima in Figure 2A. The correspondence of PC yield with molecular absorption spectrum is consistent with that observed for eight single-component MJs reported recently.[7] The PC yields for each of the respective bilayers are 8–15 times larger than either single-layer device, and have apparent features close in wavelength to the absorbance maxima of both AQ and BTB. Furthermore, the PC polarity changes upon reversing the order of BTB and AQ in the bilayer MJs. The correspondence of each PC band to the associated absorption bands in Figure 2A is further supported by the observed changes in PC yield at 360 and 300 nm for several bilayers with varying thickness of BTB and AQ shown in Figure S3 in the Supporting Information. As the AQ thickness is increased, the PC yield at 300 nm becomes increasingly prominent compared with that at 360 nm. Interestingly, as the thickness of AQ increases on top of BTB, the PC over the entire wavelength region examined decreases significantly, implying that thicknesses corresponding to ≈5–6 molecular units of AQ and BTB are near optimum for obtaining large PC yields. As noted below, possible charge transfer transitions at the AQ–BTB interface may be a significant source of the observed PC.

To better understand photon conversion into electron transport near the PC yield maximum of 360 nm, open-circuit voltage (V_{oc}) and short-circuit current density (J_{sc}) were determined during illumination by a 407 nm diode laser (10 mW, 1.25 W cm^{-2} at the sample). Initially, for all systems with the shutter closed (t = 0 to 6 s), V_{oc} and J_{sc} are below the limit of instrumental sensitivity (3×10^{-5} V, and 5×10^{-5} mA cm^{-2}). However, upon laser illumination, the V_{oc} and J_{sc} for the single layer of AQ quickly reach steady state values of −15.3 mV and −0.064 mA cm^{-2}, respectively, while a single layer of BTB alone yields +30.2 mV and +0.207 mA cm^{-2}, as summarized in **Table 1**. Reversing the order of the BTB and AQ layers causes reversal of the polarities of both V_{oc} and J_{sc}. Table 1 also includes the observed values for the same MJs with laser illumination through the bottom electrode, illustrating that the signs of the V_{oc} and J_{sc} are independent of the illumination direction. Due to the lower transparency of the bottom electrode relative to the top electrode, the J_{sc} values are observed to be consistently lower than those with light incident on the top electrode. As shown in **Figure 3**A, the observed PC is linear with laser intensity. The PC illuminated by 1.25 W cm^{-2} at 407 nm slowly

Table 1. Summary of V_{oc} and J_{sc} values measured with a 407 nm laser in different illumination directions (300 mW cm^{-2} power density).

Molecular Layer(s)[a)]	V_{oc} (top)[b)] [mV]	V_{oc} (bottom)[b)] [mV]	J_{sc} (top) [mA cm^{-2}]	J_{sc} (bottom) [mA cm^{-2}]
AQ	−15.3	−2.2	−0.064	−0.005
BTB	+30.2	+26.7	+0.207	+0.045
AQ–BTB	−188.4	−166.0	−0.493	−0.285
BTB–AQ	+394.4	+377.6	+1.548	+0.484

[a)]For the bilayers, the molecular layer grafted to the "bottom" electrode is listed first; [b)]"Top" and "bottom" indicate which electrode is illuminated.

decreased with time as shown in Figure 3B by ≈40% after an hour of constant laser exposure in ambient air. The bilayer devices exhibit much larger photo-generated V_{oc} and J_{sc} values, for example, V_{oc} = +394 mV and +1.548 mA cm^{-2} for the BTB–AQ bilayer junction. PC spectra under Xe arc illumination (0.5–18.0 mW cm^{-2}) showed no changes in shape or magnitude with repeated acquisitions over >12 h of light exposure.

A proposed mechanism for the PCs observed in bilayer MJs must account for several distinct features of the bilayers compared with IPE in thinner, single-component MJs[5e,f] or photon-assisted tunneling when a single molecular absorber is present.[7] First, the contribution of IPE to the bilayer PC must be negligible, since it should change polarity when the illumination direction is reversed, contrary to the current results (Table 1). Second, the maximum bilayer PC occurs close to the absorbance maximum of the molecular layer, but is much larger than that for single-component MJs of the same materials. Third, the PC polarity and V_{OC} depend on the alignment of molecular energy levels relative to the electrode Fermi level for single-components MJs,[7] while the bilayer PC polarity depended on the order of the two layers, and presumably the alignment of molecular orbital energies at the organic–organic interface. Fourth, the PC spectrum shape for single-layer MJs did not vary with thickness, while that for bilayers depended strongly on the relative thickness of the two layers.

Several possible optical transitions which may underlie PC generation are shown in Figure 3, for the case where the absorber is BTB (3C) or AQ (3D). The strong correlation of PC in BTB–AQ bilayer MJs with the BTB absorption maximum at 360 nm implies that a major contribution to the PC is initiated by the HOMO to LUMO transition in BTB, indicated as step 1 in Figure 3C. The resulting electron–hole pair can then dissociate to free carriers by electron transport from the BTB LUMO to the AQ LUMO (step 2), followed by charge transport and collection of the electron–hole at the contacts (step 3). Transport through the relatively thick molecular layers is likely mediated by sequential tunneling between molecular subunits with a low activation energy, as discussed recently.[11a] Dissociation and charge transport throughout the bilayer are likely driven by the photo-induced electric field indicated by the significant V_{OC} present in illuminated bilayers. A second contribution to the PC initiated by AQ absorption at ≈300 nm is shown in Figure 3D and may be responsible for the PC shoulder at 300 nm in Figure 2B and

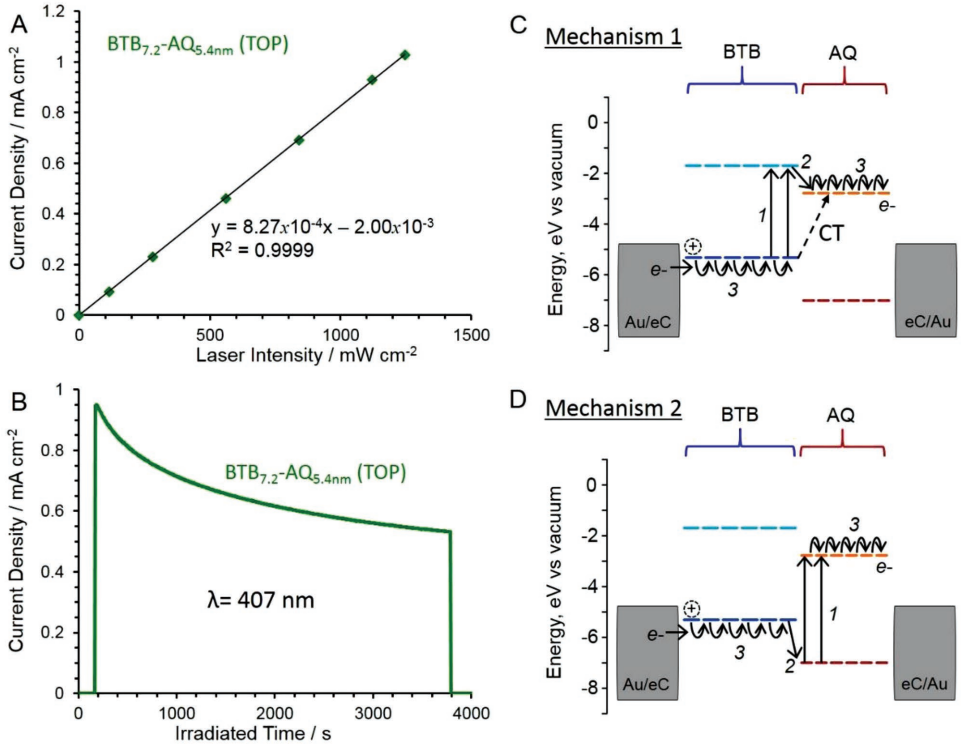

Figure 3. A) Short-circuit current density of a BTB–AQ device illuminated through the top electrode with varying power of a 407 nm laser. B) Short-circuit current density measured as a function of time the molecular junction is exposed to a 10 mW 407 nm laser (1.25 W cm^{-2}). Proposed mechanism of charge transport through C) BTB or D) AQ excitation. Energy levels were determined from DFT and do not include level shifts by electronic coupling with the contacts[11b] or between the AQ and BTB layers.

Figure S4 in the Supporting Information. Step 1 in Figure 3D is the HOMO to LUMO transition in AQ, followed by dissociation of the electron–hole pair via electron transfer from the BTB HOMO at the BTB–AQ interface. A third possible contribution is an optical charge transfer transition of an electron from the BTB HOMO to AQ LUMO indicated as "CT" in Figure 3C, with subsequent charge transport. Note that for all three contributions, the direction of charge transport does not depend on the direction of illumination, but rather on the relative energies of the molecular layers and the transitions between them. Subsequent charge transfer progresses (step 3) in the same direction as that following BTB absorption (Figure 3C). These proposed mechanisms explain the change in sign in PC yield as well as V_{OC} and J_{sc} when AQ and BTB layers are reversed in the bilayer MJ.

Time-dependent DFT (TD-DFT) provides insights into the likelihood of the proposed optical transitions shown in Figure 3 and also reveals important consequences of the bilayer structure. Figures S4 and S5 in the Supporting Information show the orbitals, energies, and oscillator strengths (f) of transitions in dimers of AQ and BTB as well as AQ–BTB and BTB–AQ, and the results are summarized in Table S1 in the Supporting Information. The HOMO of AQ–BTB is localized mainly on BTB, and the LUMO is mainly on AQ, so the H–L transition at 535 nm corresponds to the charge transfer shown in Figure 3C. However, this transition is weak ($f = 0.17$), and the small PC observed at 535 nm implies that the transition is not a significant contributor to the observed PC. Stronger transitions at 381 ($f = 1.07$) and 341 nm ($f = 0.24$) also involve significant shifts of electron density from BTB to AQ, and are likely contributors to the observed PC. While the reversed case of BTB–AQ has a different linkage between the thiophene and benzene rings, it has similar optical transitions which transfer electron density from BTB to AQ.

In conclusion, a bilayer MJ with an active layer thickness of less than 15 nm can generate PCs and open-circuit voltages much larger than those for single-layer components of similar thickness and the same molecular structures. The bilayer structure not only introduces asymmetry into the MJ by juxtaposing two sets of molecular orbital energies but also enables optical transitions which directly transfer charge between the two molecular layers. The covalent bond at the organic–organic interface[12] creates a distinct molecule with different optical and electronic properties from its components, and which may be exploited for enhancing the observed PC and changing its polarity. The direction of rectification and the PC polarity depend on the relative energies of the two molecular layers, and not on illumination direction or differences in the contact/molecule interfaces. Improvements in performance should be possible using different chromophores, optimizing thicknesses and optical path length, and designing the donor–acceptor interface for maximum photo-induced charge transfer. In addition to providing probes of internal energy levels and charge transport, photo-induced currents and voltages may potentially be useful in light-weight, durable, and flexible photodetectors.

Experimental Section

Materials and Sample Preparation: Bottom electrode contacts were patterned on diced, fused quartz chips (Quartz Unlimited LLC, nanograde polish), as shown in Figure 1B, by sequential electron beam evaporation (Kurt J. Lesker PVD75) of Cr (4 nm), Au (30 nm), and eC (10 nm, from spectroscopic grade graphite) through a shadow mask following a previously established procedure.[6c,9] AQ diazonium tetrafluoroborate was prepared and stored at 4 °C using the 2-aminoanthraquinone precursor (Sigma-Aldrich) as described previously.[9] BTB diazonium ions were prepared from the amino precursor (BTAB, synthesized at the University of Paris by Prof. Jean-Christophe et al.) in situ prior to electrochemical grafting using *tert*-butyl nitrite (Sigma-Aldrich) as an oxidizing agent.[3,9] Oligomer layers of AQ and BTB were deposited on the eC substrate by electrochemical reduction of 1×10^{-3} M diazonium ions in tetrabutylammonium tetrafluoroborate ($TBABF_4$, Sigma-Aldrich) electrolyte in acetonitrile by cyclic voltammetry using a three-electrode potentiostat (CH Instruments, CHI440) with a Pt wire counter electrode and a saturated $Ag/AgNO_3$ reference electrode. Electrochemical scan conditions are summarized in Table S2 in the Supporting Information, and the resulting molecular layers were characterized by Raman spectroscopy.[12] Top contacts of eC (10 nm) and Au (20 nm) were perpendicularly patterned over the electrochemically grafted molecular layers through a similar vapor deposition as shown in Figure 1B forming 500×250 µm molecular junctions.

Instrumental: DFT calculations were performed to predict HOMO and LUMO levels of BTB and AQ as free molecules using the B3LYP functional and 6-31G(d) basis set in the Gaussian 09 program. Absorbance spectra of molecular layers grafted to nonpatterned quartz/Cr/Au/eC samples were collected with an Agilent 8453 UV–vis spectrophotometer between 190 and 1000 nm.[9] PC experiments were collected using a Xenon arc lamp with a 150 W power source coupled with a monochromator (bandpass = 13 nm) through an optical beam chopper and focused onto the molecular junction through the top contact. A lock-in amplifier was employed for PC detection referenced to the optical beam chopper. The procedure for verification of PC direction had been previously reported.[5e] Photon power density was independently measured for each wavelength studied using a Newport 1936-R power meter for determination of the external quantum efficiency, i.e., yield. Molecular layer thicknesses were determined near molecular junctions through an atomic force microscopy scratching technique,[3,13] with a Veeco DI 3100 microscope and a silicon cantilever probe (µmasch, 325 kHz, 40 N m^{-1}, HQ:NSC15/Al BS).

Supporting Information

Supporting Information is available from the Wiley Online Library or from the author.

Acknowledgements

The authors thank the University of Alberta, the National Research Council of Canada, the Natural Science and Engineering Research Council, and the Alberta Innovates for their support, as well as Prof. Jean-Christophe Lacroix and Dr. Denis Frath at the University of Paris for providing the amino precursor for BTB diazonium ion synthesis.

Conflict of Interest

The authors declare no conflict of interest.

Keywords

all-carbon molecular junctions, bilayer rectifiers, molecular electronics, photocurrents, photovoltage

Received: February 13, 2018
Revised: March 13, 2018
Published online: April 17, 2018

[1] a) A. Vilan, D. Aswal, D. Cahen, *Chem. Rev.* **2017**, *117*, 4248; b) N. J. Tao, in *Nanoscience and Technology* (Ed. P. Rodgers), Macmillan Publishers Ltd/World Scientific Publishers, London/Singapore, **2009**, 185; c) N. A. Zimbovskaya, M. R. Pederson, *Phys. Rep.* **2011**, *509*, 1.

[2] a) A. J. Bergren, R. McCreery, S. Nagy, H. Yan, A. Bayat, M. Kondratenko, *ECS Trans.* **2014**, *61*, 113; b) R. McCreery, A. Bergren, A. Morteza-Najarian, S. Y. Sayed, H. Yan, *Farad. Discuss.* **2014**, *172*, 9; c) D. Taherinia, C. E. Smith, S. Ghosh, S. O. Odoh, L. Balhorn, L. Gagliardi, C. J. Cramer, C. D. Frisbie, *ACS Nano* **2016**, *10*, 4372; d) S. H. Choi, B. Kim, C. D. Frisbie, *Science* **2008**, *320*, 1482; e) L. Luo, L. Balhorn, B. Vlaisavljevich, D. Ma, L. Gagliardi, C. D. Frisbie, *J. Phys. Chem. C* **2014**, *118*, 26485; f) Q. v. Nguyen, P. Martin, D. Frath, M. L. Della Rocca, F. Lafolet, C. Barraud, P. Lafarge, V. Mukundan, D. James, R. L. McCreery, J.-C. Lacroix, *J. Am. Chem. Soc.* **2017**, *139*, 11913.

[3] A. Bayat, J.-C. Lacroix, R. L. McCreery, *J. Am. Chem. Soc.* **2016**, *138*, 12287.

[4] D. D. James, A. Bayat, S. R. Smith, J.-C. Lacroix, R. L. McCreery, *Nanoscale Horiz.* **2018**, *3*, 45.

[5] a) Y.-L. Loo, D. V. Lang, J. A. Rogers, J. W. P. Hsu, *Nano Lett.* **2003**, *3*, 913; b) P. Pourhossein, R. K. Vijayaraghavan, S. C. J. Meskers, R. C. Chiechi, *Nat. Commun.* **2016**, *7*, 11749; c) M. Galperin, A. Nitzan, *Phys. Chem. Chem. Phys.* **2012**, *14*, 9421; d) M. Galperin, A. Nitzan, M. A. Ratner, D. R. Stewart, *J. Phys. Chem. B* **2005**, *109*, 8519; e) J. A. Fereiro, M. Kondratenko, A. J. Bergren, R. L. McCreery, *J. Am. Chem. Soc.* **2015**, *137*, 1296; f) J. A. Fereiro, R. L. McCreery, A. J. Bergren, *J. Am. Chem. Soc.* **2013**, *135*, 9584; g) S. Ajisaka, B. Zunkovic, Y. Dubi, *Sci. Rep.* **2015**, *5*, 8312.

[6] a) U. M. Tefashe, Q. V. Nguyen, F. Lafolet, J.-C. Lacroix, R. L. McCreery, *J. Am. Chem. Soc.* **2017**, *139*, 7436; b) O. Ivashenko, A. J. Bergren, R. L. McCreery, *Adv. Electron. Mater.* **2016**, *2*, 1600351; c) O. Ivashenko, A. J. Bergren, R. L. McCreery, *J. Am. Chem. Soc.* **2016**, *138*, 722; d) W. Du, T. Wang, H.-S. Chu, L. Wu, R. Liu, S. Sun, W. K. Phua, L. Wang, N. Tomczak, C. A. Nijhuis, *Nat. Photonics* **2016**, *10*, 274.

[7] A. M. Najarian, A. Bayat, R. L. McCreery, *J. Am. Chem. Soc.* **2018**, *140*, 1990.

[8] a) J. Yu, Y. Zheng, J. Huang, *Polymers* **2014**, *6*, 2473; b) Y.-W. Su, S.-C. Lan, K.-H. Wei, *Mater. Today* **2012**, *15*, 554; c) A. Pivrikas, N. S. Sariciftci, G. Juška, R. Österbacka, *Prog. Photovoltaics* **2007**, *15*, 677; d) B. Kippelen, J.-L. Bredas, *Energy Environ. Sci.* **2009**, *2*, 251.

[9] A. Morteza Najarian, B. Szeto, U. M. Tefashe, R. L. McCreery, *ACS Nano* **2016**, *10*, 8918.

[10] A. Morteza Najarian, R. Chen, R. J. Balla, S. Amemiya, R. L. McCreery, *Anal. Chem.* **2017**, *89*, 13532.

[11] a) A. Morteza Najarian, R. L. McCreery, *ACS Nano* **2017**, *11*, 3542; b) S. Y. Sayed, J. A. Fereiro, H. Yan, R. L. McCreery, A. J. Bergren, *Proc. Natl. Acad. Sci. U. S. A.* **2012**, *109*, 11498.

[12] M. Supur, S. R. Smith, R. L. McCreery, *Anal. Chem.* **2017**, *89*, 6463.

[13] F. Anariba, S. H. DuVall, R. L. McCreery, *Anal. Chem.* **2003**, *75*, 3837.

